Application of a numerical simulation to improve the separation efficiency of a sperm sorter

**Toru Hyakutake · Yuki Hashimoto · Shinichiro Yanase ·
Koji Matsuura · Keiji Naruse**

Abstract This paper describes a study in which numerical simulations were applied to improve the separation efficiency of a microfluidic-based sperm sorter. Initially, the motion of 31 sperm were modeled as a sinusoidal wave. The modeled sperm were expected to move while vibrating in the fluid within the microchannel. In this analysis, the number of sperm extracted at the outlet channel and the rate of movement of the highly motile sperm were obtained for a wide range of flow velocities within the microchannel. By varying the channel height, and the width and the position of the sperm-inlet channel, we confirmed that the separation efficiency was highly dependent on the fluid velocity within the channel. These results will be valuable for improving the device configuration, and might help to realize further improvements in efficiency in the future.

Keywords Human reproduction · Microfluid ·
Numerical simulation · Separation efficiency · Sperm sorter

1 Introduction

Infertility is often cited as one of the causes of the declining birthrate, which has become a serious social problem in recent years. Roughly 10% of couples have infertility problems, and almost 50% of all cases of infertility are associated with a lack of sperm or sperm abnormalities (Mosher and Pratt 1991). Motile sperm are required to increase the probability of fertilization. Processes by which motile sperm can be safely and easily sorted are therefore important for infertility treatment. Currently, the swim-up method and the density-gradient centrifugal method (Smith et al. 1995) are employed for sperm sorting. However, these methods sort sperm in a non-physiological environment, so damage such as DNA fragmentation is a major problem (Younglai et al. 2001), and might result in the sorting of sperm that are unsuitable for fertilization.

Cho et al. (2003) proposed a sperm-sorting method that used a microfluidic system to extract motile sperm without physical damage, such as that caused by centrifugation. Figure 1 shows an outline of such a sperm sorter with a microfluidic system. The microchannels in the device are fabricated using soft-lithography methods (Duffy et al. 1998). Fluids flowing from two inlets (a and b) form a laminar stream as their Reynolds numbers are small. The laminar streams of the fluid flow in parallel, without mixing at the interface between the streams in order to reach outlets c and d (Brody and Yager 1997; Weigl and Yager 1999; Kenis et al. 1999; Takayama et al. 2001; Tokeshi et al. 2002; Takayama et al. 2003). If a fluid containing sperm is made to flow from inlet a, non-motile sperm and cells reach outlet c along the stream. However, some motile sperm pass through the interface to reach outlet d. Therefore, only motile sperm are extracted from outlet d. The flow is generated by a method that utilizes the head-pressure difference produced by the difference between the amounts of liquids in the reservoir chambers; therefore, compared with conventional pump systems based on mechanical methods, this device is relatively simple and convenient to

T. Hyakutake (✉) · Y. Hashimoto · S. Yanase
Graduate School of Natural Science and Technology,
Okayama University,
3-1-1, Tsushimanaka,
Okayama 700-8530, Japan
e-mail: hyaku@mech.okayama-u.ac.jp

K. Matsuura · K. Naruse
Graduate School of Medicine,
Dentistry and Pharmaceutical Sciences, Okayama University,
2-5-1, Shikata-cho,
Okayama 700-8558, Japan
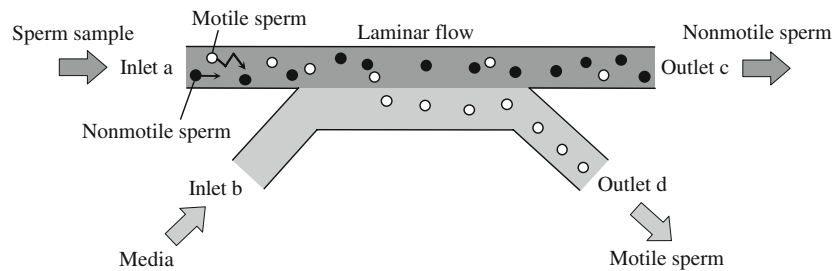
Fig. 1 Schematic diagram of a sperm sorter (Cho et al. 2003). When fluid containing sperm was made to flow from *inlet a*, the non-motile sperm and cells reached *outlet c* along the stream. However, some motile sperm passed through the interface to reach *outlet d*. Therefore, only motile sperm exited from *outlet d*

use. This is an important advantage, given that the device is likely to be employed by many individuals at various clinical sites. Schuster et al. (2003) have investigated parallel streams with width ratios 1:3 and discussed the influence of the flow rate, duration of contact between the parallel streams, and width of inlets on device efficiency. However, the device shape or hydrodynamic conditions that will allow the extraction of motile sperm with maximum efficiency have not yet been investigated in detail. Consequently, inexpensive and immediately executable numerical simulations are required to estimate the separation efficiency of sperm sorters. Furthermore, optimally configured devices also need to be investigated.

Various flagellar models of sperm motion have been proposed (Gray and Hancock 1955; Rikmenspoel 1978; Higdon 1979). The curvilinear velocity and the amplitude of motion are important from the viewpoint of investigating the separation efficiency of motile sperm. The present study therefore modeled sperm motion as a simple sinusoidal wave, as shown in Fig. 2(a). In the simulation, the modeled sperm were arranged at either inlet of the sperm sorter, in order to enable them to move while vibrating in the fluid within the microchannel. This paper describes how variations in the height of the microchannel and the width of the

sperm-inlet channel affected the number of motile sperm extracted at outlet d. In addition to the existing two-inlet, two-outlet microfluidic channel, a three-inlet, three-outlet microfluidic channel system was analyzed, and the separation efficiency of the motile sperm was compared between the two systems. It is hoped that the separation characteristics of sperm sorters with microfluidic systems will be clarified through these analyses, and that the knowledge gained will allow such devices to be improved in the future.

2 Methods

2.1 Modeling of sperm motion

In the present study, 31 sperm from an adult male were used to construct a sperm motion model. The sperm motion was hypothesized to be a sinusoidal wave, as shown in Fig. 2(a). Therefore, in order to model the motion, it was necessary to determine the sperm velocity, the amplitude of the sinusoidal wave, and the period. First, an animation of 60 fps obtained by microscopy was analyzed using MATLAB digital image-analysis software (The Mathworks, Inc.) to obtain the locus of the sperm motion. Figure 2(b)

Fig. 2 (a) Sperm motion modeled as a sinusoidal wave. The amplitude is denoted by A and the straight-line length is denoted by L_X. (b) Motion tracking of a sample sperm plotted on a graph. When an axis obtained by the least-squares method was specified as the X-axis, the difference between the maximum and minimum values of the Y-coordinate was defined as twice the amplitude A
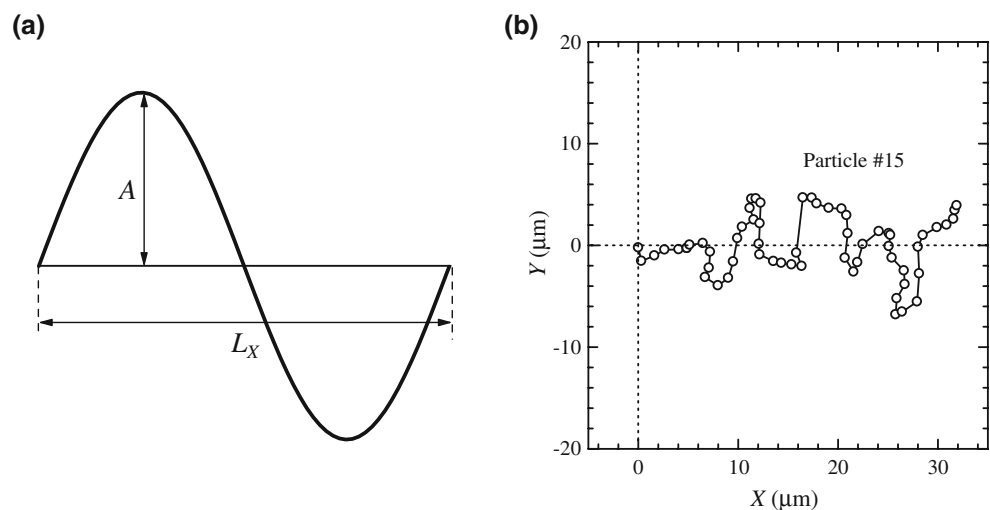
shows an example of the results of tracking the motion of a sample sperm. By specifying an axis obtained by the least-squares method as the X-axis, the difference between the maximum and minimum values of the Y-coordinate was defined as twice the amplitude A. As sperm are subjected to high viscosity in a low Reynolds number environment, a driving force can be obtained by inducing high-speed vibrations using flagella.

All 31 sperm were subjected to this processing, and the motion was modeled based on the results. Initially, the length S of the sinusoidal wave shown in Fig. 2(a) was expressed as follows when applying a complete elliptic integral, and using the amplitude A and the straight-line length L_X of one period:

$$S = \sqrt{\left(\frac{L_X}{2\pi}\right)^2 + A^2} \frac{\pi}{2(1+\alpha)}\left(1 + \frac{1}{4}\alpha^2\right),$$

$$\alpha = \frac{\sqrt{1+k^2}-1}{\sqrt{1+k^2}+1}. \tag{1}$$

Here, $k=2\pi A/L_X$ and higher-order terms are omitted. When representing S and L_X in terms of the sperm velocity V, the straight-line velocity V_X, and the period T used in the present analysis, the following expressions were obtained:

$$S = VT, \quad L_X = V_X T. \tag{2}$$

From the results of the analysis of the sample sperm, the sperm velocity V and the period T were determined as follows:

$$V = V_{max}R, \tag{3}$$

$$T = T_{av}. \tag{4}$$

Here, R denotes a random number. $V_{max}=100$ μm/s was the maximum velocity in the sample sperm. Therefore, the V of the modeled sperm was distributed uniformly in the range of 0–100 μm/s. The mean period of the 31 sperm was $T_{av}=$ 0.355 s. Accordingly, by substituting Eqs. 2–4 into Eq. 1, the relation between the amplitude A and the straight-line velocity V_X could be obtained. A and V_X were randomly determined within the range of the sample sperm data, so as to satisfy this relation. With regard to the motility, sperm with a velocity that was more than 50% of the V_{max} were judged to be highly motile.

2.2 Analysis of sperm motion within microchannels

Figure 3(a) and (b) shows schematic diagrams of the two sperm sorters investigated in the present study: a two-inlet, two-outlet microfluidic channel and a three-inlet, three-outlet microfluidic channel, respectively. In this paper, the channel branches of the inlet and outlet were not involved in the computational domain; only the portion where the flow ran in parallel was considered. This area was assumed to be a rectangular channel flow. Assuming that the x-axis was the flow direction and that the yz-plane was a rectangular cross-section (Fig. 3(c)), the velocity distribution in the cross-section could be theoretically obtained as follows (White 1991):

$$
\begin{aligned}
u_x(y,z) &= \frac{16a^3}{\pi^3\mu}\frac{\partial p}{\partial x}\sum_{n=1,3,5,\cdots}^{\infty}\frac{1}{n^3}(-1)^{\frac{n-1}{2}}\left(1 - \frac{\cosh\frac{n\pi y}{2a}}{\cosh\frac{n\pi b}{2a}}\right)\cos\frac{n\pi z}{2a} \\
&= \frac{\pi b u_m}{2}\frac{\displaystyle\sum_{n=1,3,5,\cdots}^{\infty}\frac{1}{n^3}(-1)^{\frac{n-1}{2}}\left(1-\frac{\cosh\frac{n\pi y}{2a}}{\cosh\frac{n\pi b}{2a}}\right)\cos\frac{n\pi z}{2a}}{\displaystyle\sum_{n=1,3,5,\cdots}^{\infty}\frac{1}{n^4}\left(b-\frac{a}{n\pi}\tanh\frac{n\pi b}{2a}\right)}.
\end{aligned}
\tag{5}
$$

Here, u_m denotes the mean flow velocity in the rectangular channel. From Eq. 5, when the shape of the channel cross-section and u_m were known, the flow-velocity distribution within the channel could be obtained. The left-hand side of Fig. 3(c) shows the flow-velocity distribution in the cross-section of the rectangular channel, and the right-hand side of Fig. 3(c) shows the flow-velocity distribution at $z=0$ when $a=$ 250 μm, $b=500$ μm, and $u_m=1000$ μm/s as an example. The flow velocity was highest at the center, and decreased as the liquid approached the wall surface due to the viscosity. As the flow was sufficiently laminar within the actual micro-channel, the flow-velocity distribution was thought to be similar to that given by Eq. 5, except in the portions where the flow branched. The sperm modeled in the previous section were arranged at the upstream side of the sperm-inlet channel, and the sperm motion was considered as follows:

$$
\begin{aligned}
x^{t+\Delta t} &= x^t + \Delta x_s + u(y^t, z^t)\Delta t, \\
y^{t+\Delta t} &= y^t + \Delta y_s, \\
z^{t+\Delta t} &= z^t + \Delta z_s.
\end{aligned}
\tag{6}
$$

Here, Δx_s, Δy_s, and Δz_s are the distances that the modeled motile sperm moves as a sinusoidal wave along the x, y, and z directions, respectively, in Δt when there is no flow. The initial direction of the straight-line velocity of the sperm was randomly specified in all directions. In the present analysis, the influence of sperm motion on the fluid and the mutual interference between sperm were neglected. It was assumed that when a sperm collided against a wall, it would be reflected diffusely.

The microchannel length L and width W were fixed as 5000 μm and 500 μm, respectively, while the channel height H was varied. The number of all of the modeled sperm that were made to flow was $N_0=1\times10^4$ and the volume of the inflow liquid was $C_f=5$ cm^3, with this number being constant. As shown in Fig. 3(a) and (b), the A-channel connected the sperm inlet and the non-motile-sperm outlet, and the B-channel connected the sperm-free media inlet and the motile-sperm outlet. In the case of three-inlet, three-outlet channels,

there were two types of B-channels at the top and bottom. The width of the A-channel was W_A and that of the B-channel was W_B. The number of sperm arriving at the A-channel outlet, the non-motile-sperm outlet, was N_A. The number of sperm arriving at the B-channel outlet, the motile-sperm outlet, was N_B. Among the sperm arriving at the B-channel outlet, the number judged to be highly motile ($V > 0.5V_{max}$) was N_B^G. The time t necessary to make an amount of liquid (C_f) flow

completely varied according to differences in the water-head pressure of the microchannel and differences in the wettability of the channel surface. In other words, the u_m within the channel varied extensively according to the device setup. Accordingly, in the present calculation, the influence of the change of H and W_A/W on N_B and N_B^G was investigated for a wide range of flow velocities within the channel. Moreover, the difference between the two-inlet, two-outlet microfluidic

Fig. 3 (a) Two-inlet, two-outlet microfluidic channel. (b) Three-inlet, three-outlet microfluidic channel. The channel branches were not involved in the computational domain, and only the portion where the flow ran in parallel was considered. It was assumed that this area was a rectangular channel flow. (c) The figure on the left-hand side shows the flow-velocity distribution in a cross-section of the rectangular channel, and the figure on the right-hand side shows the flow-velocity distribution at $z=0$ when $a=250$ μm, $b=500$ μm, and $u_m=1000$ μm/s as an example
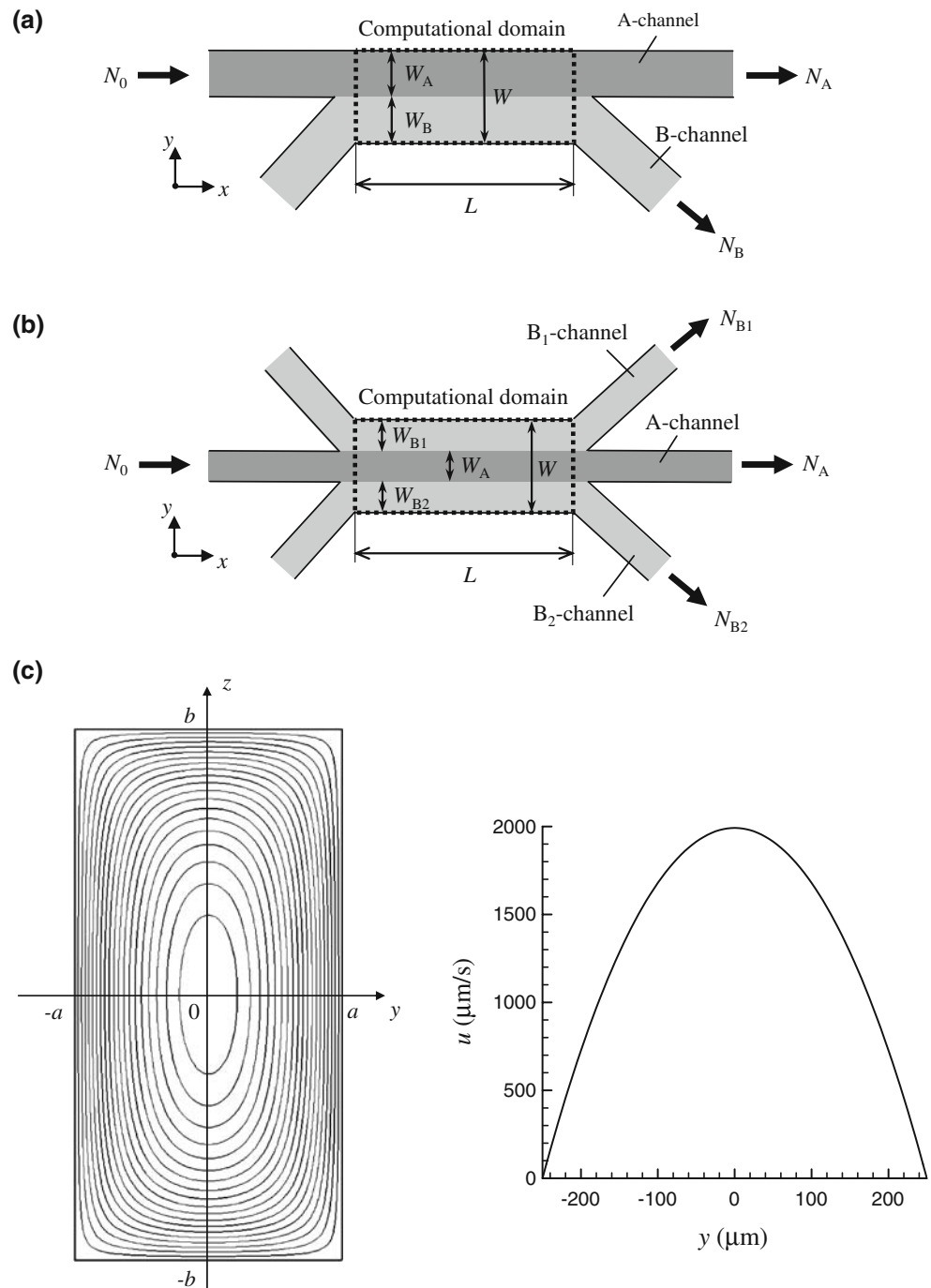
channel and the three-inlet, three-outlet microfluidic channel was examined.

In practice, the viscosity of fluid in inlet a is slightly higher than that of inlet b, although semen flowing from inlet a is diluted in order to decrease its viscosity. The actual flow rate in the A-channel may therefore be lower than the numerically calculated flow rate; as a result of the discrepancy in flow rates between the A and B channels, the A channel is made more narrow as fluid from the B channel encroaches into the space parallel. However, the thinning of the A-channel stream does not lead to the movement of non-motile sperm and cells from inlet a to outlet d, and the separation efficiency between the streams remains almost identical. If the deviation in the flow rate is large, the flow rate can be adjusted manually. Consequently, in the present simulation, the influence of semen viscosity on the flow rate in the channels and the separation characteristics are not considered.

3 Results and discussion

3.1 Effect of H

Initially, the sperm-sorting characteristics of the two-inlet, two-outlet microfluidic channel were investigated. This section shows the separation efficiency when W_A/W was set to 0.25 and the height of the microchannel was varied. Figure 4(a) and (b) shows the change in the N_B of sperm and the N_B^G of motile sperm arriving at the B-channel versus the u_m within the microchannel, respectively. The u_m was approximately 1.0×10^3 μm/s for the present device. Therefore, for example, when $H = 1000$ μm, the Reynolds number within the channel was Re$= u_m W / \nu = 0.5$, where ν denotes the kinematic viscosity ($\nu = 1.0$ mm^2/s) and the time required for 5 cm^3 of liquid to flow completely was $t = C_f / (W \cdot H \cdot u_m) = 10,000$ s. Figure 4(a) and (b) shows that as the u_m became slower, the total numbers of sperm and motile

Fig. 4 Separation efficiency when W_A/W was set to 0.25 and the microchannel height H was varied (500, 1000, and 2000 μm). (a) N_B of sperm arriving at the B-channel versus u_m within the channel. (b) N_B^G of highly motile sperm. (c) N_B^G/N_B of highly motile sperm
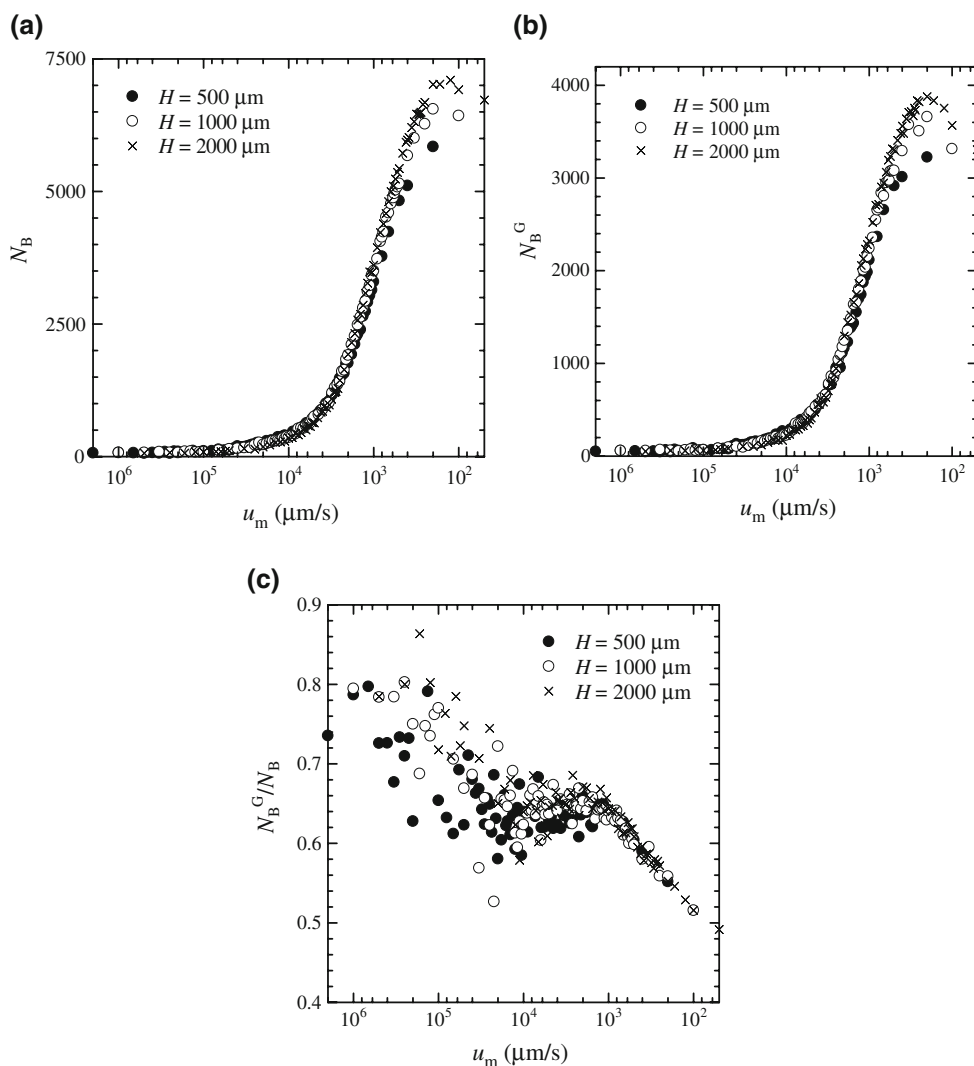
sperm sorted into the B-channel increased. This was due to the fact that the lower the u_m was, the longer the sperm remained within the channel, and thus the probability that the motile sperm passed through the interface between the channels increased. However, when the u_m became lower than a certain velocity, the number of sperm arriving at the B-channel reached a constant value, as the sperm became almost uniformly distributed within the channel.

A large H caused an increase in the interface area between the two channels. However, there was little change in N_B between different H values. Thus, the probability that the motile sperm passed through the interface between the channels was dependent largely on u_m rather than H. Accordingly, regardless of the channel depth, the number of sperm that could be extracted into the B-channel could be estimated if the u_m within the channel was known. In the present analysis, the amount of inflow liquid was assumed to be constant; therefore, if the volume of inflow liquid along with the channel depth was increased, the N_B

inevitably increased in proportion to the volume of inflow liquid and the channel depth.

The variation of N_B^G/N_B for wide ranges of u_m is shown in Fig. 4(c). When u_m was large, the probability that the sperm might cross the interface between channels decreased; as a result, there was large variation in the data. As only sperm with high motility could cross the interface at high u_m, the value of N_B^G/N_B tended to increase. However, little influence of differences in H on N_B^G/N_B was observed. Therefore, N_B^G/N_B appeared to depend largely on u_m, as well as the N_B of sperm arriving at the B-channel.

3.2 Effect of A-channel width

The results of changing the ratio W_A/W of the width of the A-channel were as follows. Figure 5(a) and (b) shows the change of N_B and N_B^G, respectively, for different values of u_m within the channel. As the channel cross-section did not

Fig. 5 Separation efficiency when W_A/W was varied (1/2, 1/5, 1/10, and 1/50). (a) u_m within the channel (or time t required for complete flow) versus N_B of sperm arriving at the B-channel. (b) N_B^G of highly motile sperm. (c) N_B^G/N_B of highly motile sperm
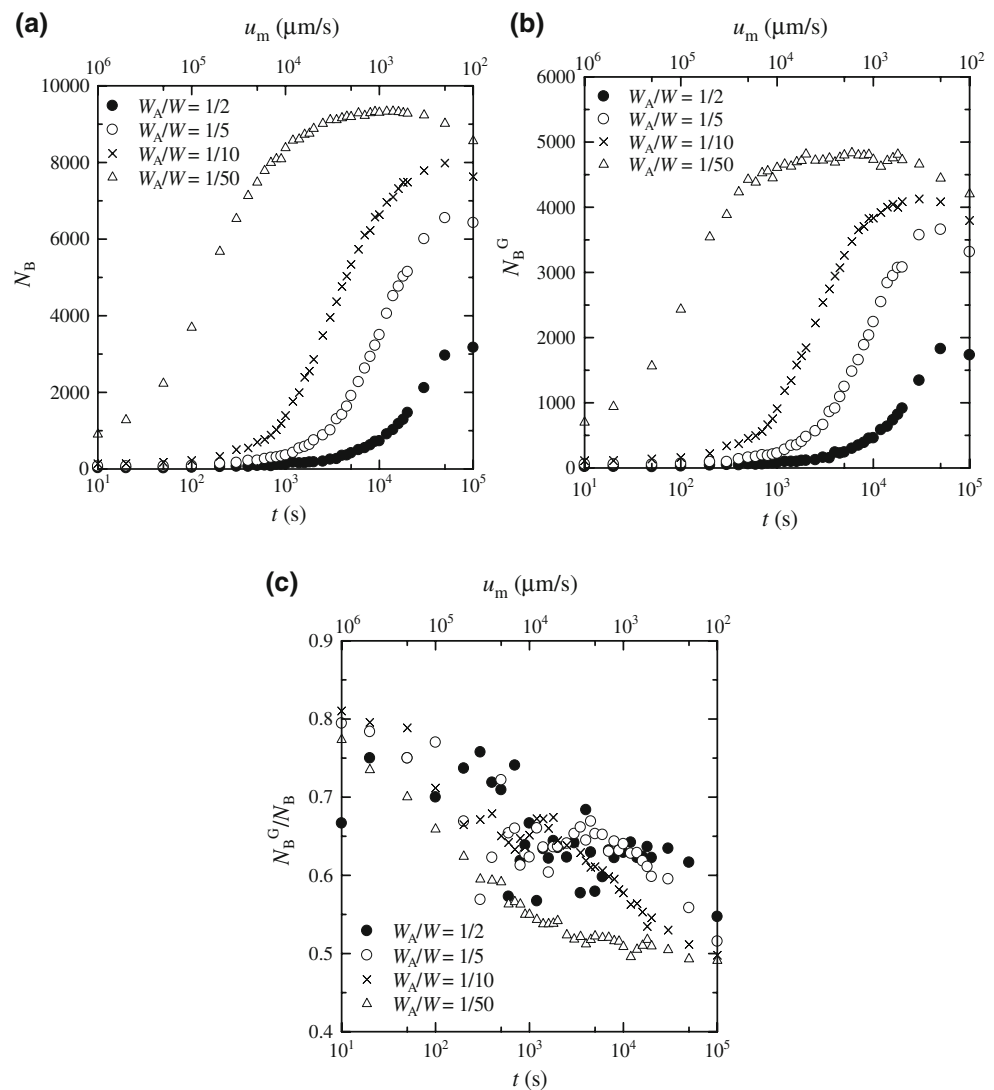
Fig. 6 Comparison of a conventional two-inlet, two-outlet microfluidic channel with a three-inlet, three-outlet microfluidic channel, in which the A-channel was in the center. (a) u_m within the channel (or time t required for complete flow) versus N_B of sperm arriving at the B-channel. (b) N_B^G of highly motile sperm. (c) N_B^G/N_B of highly motile sperm
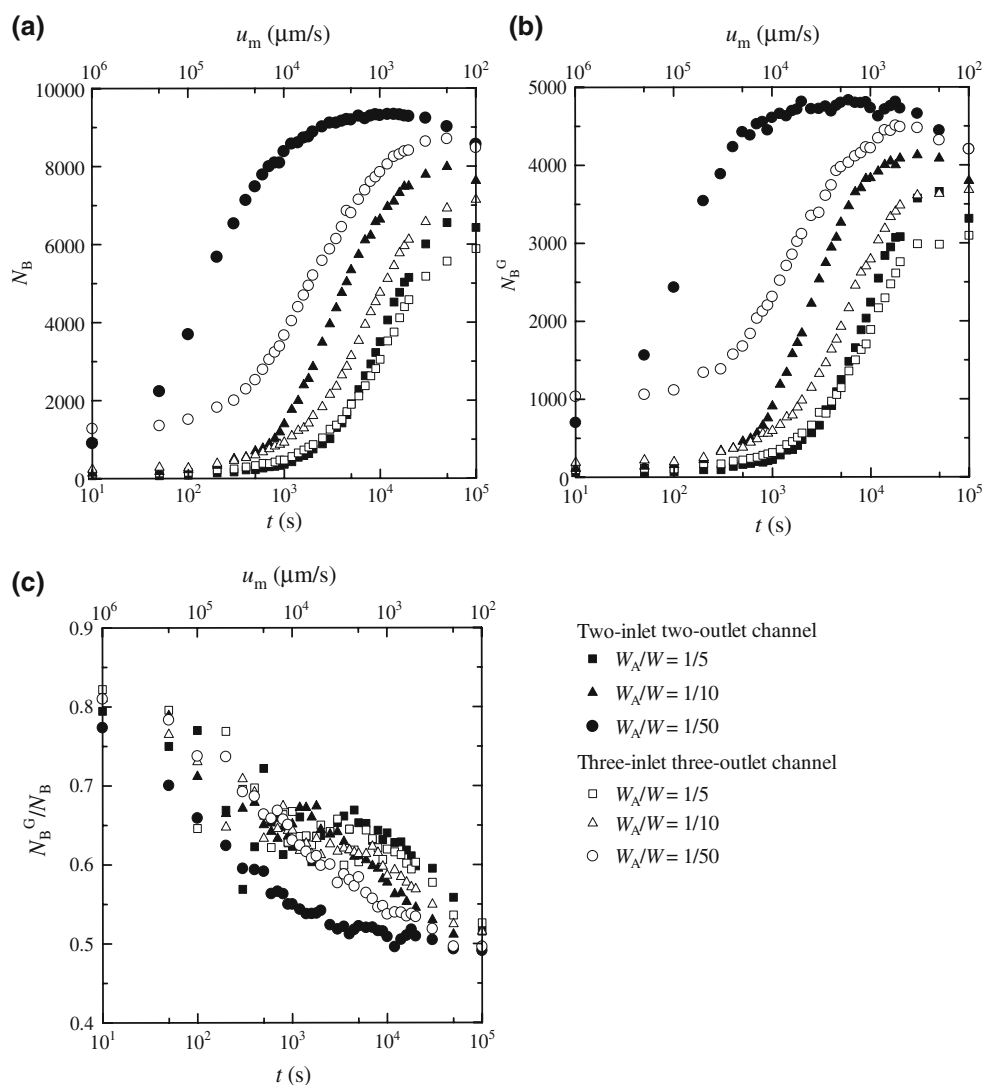
change, u_m and t corresponded to the scales at the top and bottom of the graph, respectively. When W_A/W was small, the u_m in the A-channel was slow in comparison to the u_m of the entire channel. Therefore, a small W_A/W value increased the probability that the motile sperm would pass through the interface between the A-channel and the B-channel, and the N_B increased accordingly. However, as W_A/W decreased, a processing limit was reached. Smaller dimensions of W_A lead to a significant decrease in the flow rate within inlet A, ultimately causing the sorting operation to become unreasonably long. Therefore, in reality, it will be necessary to maintain the channel width to some extent.

Figure 5(c) shows the N_B^G/N_B of the sperm that were judged to be highly motile compared to those arriving at the B-channel. Similar to in Fig. 4(b), a tendency was observed wherein N_B^G/N_B increased with u_m. However, the u_m in the A-channel decreased with W_A/W; thus, the probability that low-motility sperm crossed the interface increased and, consequently, the N_B^G/N_B decreased with the W_A/W. In summary, if a large number of sperm were required, the sperm-inlet channel width needed to be decreased. By contrast, the opposite treatment—namely increasing the channel width—was effective for increasing the proportion of sperm with high motility among those that were extracted.

3.3 Effect of position of A-channel

Finally, we present the sorting characteristics of the three-inlet, three-outlet microfluidic channel, in which the A-channel was located at the center. The configuration of the three-inlet, three-outlet microfluidic channel, as shown in Fig. 3(b), was as follows. The B_1-channel and the B_2-channel were fixed at the top and the bottom, with the A-channel in the center. Therefore, the interface area at which the A-channel made contact with the other channels was substantially larger—namely, twice that of the two-inlet, two-outlet microfluidic channel. The number of sperm to be

extracted was $N_B=N_{B1}+N_{B2}$. Figure 6(a) and (b) shows the changes in the N_B and N_B^G arriving at the B_1-channel and the B_2-channel against the flow time (or the u_m within the channel). Comparing the results for the two-inlet, two-outlet microfluidic channel with those for the three-inlet, three-outlet microfluidic channel, it was obvious that the N_B and N_B^G decreased for the same u_m, although the interface area was doubled in the three-inlet, three-outlet channel. These results might appear to be contradictory; however, they can be understood if one considers the flow-velocity distribution in the cross-section of the rectangular channel shown in Fig. 3(c). Even if the u_m in a given channel remained the same, by arranging the A-channel at the center, the flow velocity in the A-channel became considerably larger than that in the two-inlet, two-outlet microfluidic channel. Consequently, the probability that motile sperm passed through the interface was greatly reduced. Therefore, even if the interface area was doubled, the N_B and N_B^G decreased.

Figure 6(c) illustrates a comparison of the two-inlet, two-outlet channel with the three-inlet, three-outlet channel with regard to the N_B^G/N_B of sperm with high motility. In particular, when W_A/W was small, as the flow velocity in the A-channel was faster in the three-inlet, three-outlet channel than in the two-inlet, two-outlet channel, highly motile sperm alone could cross the interface. As a result, the N_B^G/N_B increased. Therefore, we concluded that—in the same manner as in the two-inlet, two-outlet microfluidic channel—the most important factor with regard to the number of motile sperm was the flow velocity in the A-channel. When the flow velocity increased, the total numbers of extracted sperm and motile sperm decreased; however, the ratio of the sperm with high motility increased. The highest priority when designing a sperm sorter is to remove non-motile sperm, which are assumed to hinder fertilization, and to extract as many motile sperm as possible. Accordingly, based on the results of the current analysis, a channel configuration that makes the flow velocity in the A-channel as slow as possible within the processing limits will be effective for increasing the number of extracted motile sperm.

4 Conclusions

In the present study, sperm modeling was used to predict the separation efficiency of a sperm sorter. This model was applied to analyze the motion of sperm within a microchannel, and the separation efficiency was investigated for various channel configurations. The main findings are summarized below.

The separation efficiency of highly motile sperm remained relatively unchanged if the u_m within the micro-

channel remained the same. It was therefore possible to roughly predict the separation efficiency of the device by measuring the u_m within the channel. As the width of the channel in which the sperm flowed decreased, the number of extracted motile sperm increased, while the ratio of highly motile sperm decreased. In the case of the three-inlet, three-outlet microfluidic channel, in which the A-channel was in the center, the A-channel was located at the fastest part of the rectangular channel flow-velocity distribution; therefore, although the size of the interface doubled, the number of extracted motile sperm decreased. By contrast, the ratio of the highly motile sperm increased.

These results will be valuable to help improve the device configuration, and to develop more effective sperm sorters in the future. As the present device requires neither electrical force nor other external forces, and handles sperm within a mechano-physiological environment, it is possible to apply it safely to cells other than sperm, as well as to microorganisms. We therefore propose that the present numerical simulation will predict the microorganism separation efficiency based on corresponding microorganism-motion models, and expect the technique to have wide-ranging applications, including in the field of biomedicine.

References

J.P. Brody, P. Yager, Diffusion based extraction in a microfabricated device Sens. Actuators A. **58**, 13–18 (1997) doi:10.1016/S0924-4247(97)80219-1

B.S. Cho, T.G. Schuster, X. Zhu, D. Chang, G.D. Smith, S. Takayama, Passively driven integrated microfluidic system for separation of motile sperm Anal. Chem. **75**, 1671–1675 (2003) doi:10.1021/ac020579e

D.C. Duffy, J.C. McDonald, O.J. Schueller, G.M. Whitesides, Rapid prototyping of microfluidic systems in poly(dimethylsiloxane) Anal. Chem. **70**(23), 4974–4984 (1998) doi:10.1021/ac980656z

J. Gray, G.J. Hancock, The propulsion of sea-urchin spermatozoa J. Exp. Biol. **32**, 802–814 (1955)

J.J.L. Higdon, The hydrodynamics of flagellar propulsion J. Fluid Mech. **90**(4), 685–711 (1979) doi:10.1017/S0022112079002482

P.J.A. Kenis, R.F. Ismagilov, G.M. Whitesides, Microfabrication inside capillaries using multiphase laminar flow pattering Science **285**, 83–85 (1999) doi:10.1126/science.285.5424.83

W.D. Mosher, W.F. Pratt, Fecundity and infertility in the United States: incidence and trends Fertil. Steril. **56**, 192–193 (1991)

R. Rikmenspoel, The equation of motion for sperm flagella Biophys. J. **23**, 177–206 (1978)

T.G. Schuster, B. Cho, L.M. Keller, S. Takayama, G.D. Smith, Isolation of motile spermatozoa from semen samples using microfluidics Reprod. Biomed. Online **7**, 73–79 (2003)

S. Smith, S. Hosid, L. Scott, Use of postseparation sperm parameters to determine the method of choice for sperm preparation for assisted reproductive technology Fertil. Steril. **63**, 591–597 (1995)

S. Takayama, E. Ostuni, P. LeDuc, K. Naruse, D.E. Ingber, G.M. Whitesides, Subcellular positioning of small molecules Nature **411**, 1016 (2001) doi:10.1038/35082637

S. Takayama, E. Ostuni, P. LeDuc, K. Naruse, D.E. Ingber, G.M. Whitesides, Selective chemical treatment of cellular microdomains using multiple laminar streams Chem. Biol. 10, 123–130 (2003) doi:10.1016/S1074-5521(03)00019-X

M. Tokeshi, T. Minagawa, K. Uchiyama, A. Hibara, K. Sato, H. Hisamoto et al., Continuous-flow chemical processing on a microchip by combining microunit operations and a multiphase flow network Anal. Chem. 74, 1565–1571 (2002) doi:10.1021/ac011111z

B.H. Weigl, P. Yager, Microfluidic diffusion-based separation and detection Science 283, 346–347 (1999) doi:10.1126/science.283.5400.346

F.M. White, Viscous Fluid Flow, 2nd edn. (McGraw-Hill, New York, 1991)

E.V. Younglai, D. Holt, P. Brown, A. Jurisicova, R.F. Casper, Sperm swim-up techniques and DNA fragmentation Hum. Reprod. 16 (9), 1950–1953 (2001) doi:10.1093/humrep/16.9.1950